Theory of Doping: Monovalent Adsorbates

B. Sachs[1], T. O. Wehling[1], A. I. Lichtenstein[1] and M. I. Katsnelson[2]

[1] *I. Institut für Theoretische Physik, Universität Hamburg, Jungiusstraße 9,*
D-20355 Hamburg
[2]*Radboud University of Nijmegen, Institute for Molecules and Materials,*
Heijendaalseweg 135,
6525 AJ Nijmegen
[1]*Germany*
[2]*The Netherlands*

1. Introduction

The discovery of graphene (Novoselov et al., 2004) and its remarkable electronic properties (Castro Neto et al., 2009; Geim & Novoselov, 2007; Katsnelson, 2007) initiated great research interest in this material. Particularly prospective for applications is its extraordinarily high charge carrier mobility (Bolotin et al., 2008; Du et al., 2008; Novoselov et al., 2004).

Realistic graphene samples are subject to disorder including ripples, impurities, edges or strains. While these present undesirable obstacles when trying to minimize electron scattering, controlled external perturbations recently evoked broad interest in the context of functionalization of graphene (Elias et al., 2009).

Impurities on a graphene sample are imaginable in various ways. While lattice imperfections like vacancies do not exist in noticeable concentrations unless they are not created artificially (Chen et al., 2009), adatoms or molecules from the experimental environment can be seen as a frequent source of electron scattering. The impact of adsorbate-induced scattering processes on the transport properties has been subject of ongoing discussion since the first fabrication of single graphene sheets in 2004 (see Peres (2010) for a review).

Transport experiments with chemically doped graphene samples yield different results regarding the strength of electron scattering due to the dopants: While room temperature experiments with NO_2, e.g., reported chemical doping without significant loss of carrier mobility (Schedin et al., 2007), the deposition of K at cryogenic temperatures clearly reduced the electron mobility (Chen et al., 2008). Correspondingly, the role of charged impurity scattering as compared to, e.g., scattering by resonant impurities or ripples has been controversially debated: Depending on experimental details both, charged impurities (Adam et al., 2007; Chen et al., 2008; Hwang et al., 2007; Nomura & MacDonald, 2006; Tan et al., 2007), as well as resonant impurities were discussed as dominant scattering sources (Katoch et al., 2010; Katsnelson & Novoselov, 2007; Ni et al., 2010; Ostrovsky et al., 2006; Stauber et al., 2007). Understanding charge redistributions in realistic graphene-adsorbate systems is hence crucial.

The high sensitivity of graphene to adsorbate-induced doping has been proven in numerous experiments (Bostwick et al., 2006; Ohta et al., 2006; Zhou et al., 2008). The two-dimensional nature maximizes surface effects, which even allows the detection of single adsorption events.

Using exfoliated graphene on a SiO_2 substrate with Ti/Au contacts, Schedin et al. (2007) visualized events of single molecule adsorption on graphene. Recently developed gas sensors (Collins et al., 2000; Kong et al., 2000; Robinson, Perkins, Snow, Wei & Sheehan, 2008) raise hope for a future realization of marketable single molecule detectors.

The natural concentration of impurities in graphene devices depends crucially on the sample preparation and the experimental setup. Meyer et al. (2008) reported the detection of single hydrogen adsorbates on graphene on a SiO_2 substrate by transmission electron microscopy (TEM). Under atmospheric conditions at room temperature they estimated the adsorbate concentration to 0.3%, which relates to about one impurity per $10nm^2$.

Especially hydrogenation, as demonstrated by Elias et al. (2009), provides a good prospect for controlled design of graphene's electronic properties. Hence, there is wide interest in fractionally and fully hydrogenated graphene, the *graphane*. Attaching hydrogen on graphene from both sides leads to a change from sp^2 to sp^3 hybridization, which opens a band gap. Through annealing, hydrogenation turns out to be reversible, i.e. the electronic properties of pristine graphene can be restored. Several theoretical works (Lebègue et al., 2009; Liu & Shen, 2009; Sofo et al., 2007) found a band gap of *graphane* between 3.5eV and 5.4eV. While this is slightly too high for electronic applications, partially hydrogenated graphene might be useful (Xiang et al., 2009). Hence, understanding of the adsorption mechanisms of atomic hydrogen is essential in search of new paths towards functionalization.

Equally, fluorination of graphene promises a route towards a graphene-based wide band gap semiconductor (Cheng et al., 2010; Nair et al., 2010; Robinson et al., 2010). At coverages of 70% or more, graphene-fluorine systems with reversible modification of the conductivity by several orders of magnitudes has been achieved.

Motivated by these recent and promising experiments on impurity effects in graphene, a theoretical investigation of doping effects in graphene is given in this chapter; in particular, monovalent adsorbates are considered. Extensive density functional theory (DFT) calculations are presented to derive a theory of doping and charge redistributions in graphene and to identify simple models describing these effects realistically. We concentrate on two issues: charge transfer as relevant for doping, i.e. changes in the number of mobile carriers, as well as charge transfer as relevant for Coulomb scattering. For hydrogen, fluorine, hydroxyl, chlorine and potassium adsorbates we determine the amount of the charge transfer by means of different electrostatic models and compare to band structure based methods (section (3)). Furthermore, by means of a tight-binding model, impurities are illustrated to lead to long-range doping of graphene such that even ultra-low concentrations of contamination do affect the carrier concentration. We investigate the effects of long range Coulomb interaction in this context and show that the Coulomb repulsion plays a minor role in the process of charge redistribution for impurity concentrations higher than 0.007%.

2. Calculation of charge transfer

The investigation of adsorption processes rises the question of the doping and Coulomb scattering due to single adsorbates. For instance, theoretical transport calculations predict a strong dependence of the scattering cross section on the amount of charge transferred between adsorbates and graphene (Robinson, Schomerus, Oroszlány & Fal'ko, 2008). A priori charge transfer is an ambiguous quantity as it comes back to defining the spacial extent of individual

atoms within a solid. Therefore, several concepts for the description of charge transfer will be taken into consideration, carefully compared and their implications for experimental observables like doping or scattering properties will be discussed.

2.1 Population analysis and partitioning of the electron density

A widely employed class of approaches to charge transfer analysis like the Mulliken, Bader or Hirshfeld analysis aims at directly partitioning the electronic charge density among the atoms of the system. To this end, a DFT calculation is performed which yields the electronic density and the Kohn-Sham wave functions. Partitioning schemes using projections of the Kohn-Sham wavefunctions onto localized atomic orbitals (Löwdin or Mulliken analysis, see, e.g., Segall et al. (1996)) as well as schemes dealing with the electronic density (Hirshfeld or Bader analysis, see, e.g., Meister & Schwarz (1994)) have been employed in the context of graphene adsorbate systems. While ionically bond systems are likely well suited to be correctly described by this kind of charge transfer analysis, the interpretation of Mulliken, Bader or Hirshfeld charges in physisorbed graphene-impurity systems (Leenaerts et al., 2008) or strongly covalent systems (see section 3.2) can be ambiguous. In the latter case, e.g., charge is smeared out in covalent bonds, and therefore a partition of the interstitial region in solids is hard.

In general, we expect conventional space partition methods to be more precise for ionic than for covalent adsorbates. The Bader analysis (Bader, 1991) of covalently and ionically bond adatoms presented in sections 3.1 and 3.2 will confirm this presumption. On that account, methods to obtain charge transfer based on electrostatic potentials or the band structure will be explained in the following.

2.2 Electrostatic approaches to charge transfer

An alternative way to describe the amount of charge transfer is to utilize electrostatic models and to apply them on output from electronic structure methods like density functional theory. In this sense, the DFT results can be seen as "experimental data" being analysed by theoretical tools and models.

The DFT calculations presented, here, were performed by means of the Vienna Ab-initio Simulation Package (Kresse & Furthmüller, 1996a;b) (VASP) with PW91-GGA functionals; the geometric structure was modelled by a three-dimensional supercell and an interlayer spacing of about 25Å in order to prevent interaction. The Brillouin zones were sampled within the tetrahedron and the Methfessel-Paxton method in combination with carefully chosen k-meshes and cut-off energies. Geometries were relaxed until all forces were smaller than 0.02eV/Å per atom.

Electrostatic potential landscapes, experimentally investigated on graphene in EFM experiments (Moser et al., 2008), can be extracted from DFT simulations (Fig. 1, left) and used to determine impurity induced charge transfer. From the point of view that (doped) graphene is metallic, the sheet can be considered as a grounded metal plate of infinite size, such that — in the simplest model — charged adsorbates can be described by means of an image charge model: the adatoms are assumed as partial point charges which induces image charges in graphene. This model is valid at length scales above the screening length of the doped graphene sheet (Katsnelson (2006)). Then, the electrostatic potential, $V(r)$, in the vacuum region above the graphene sheet and the impurity can be modelled as

$$V(\vec{r}) = V_e(z) + \frac{1}{4\pi\epsilon_0} \sum_{i=1} q_i \left[\frac{1}{|\vec{r} - \vec{r}_i|} - \frac{1}{|\vec{r} - \vec{r}'_i|} \right]. \tag{1}$$
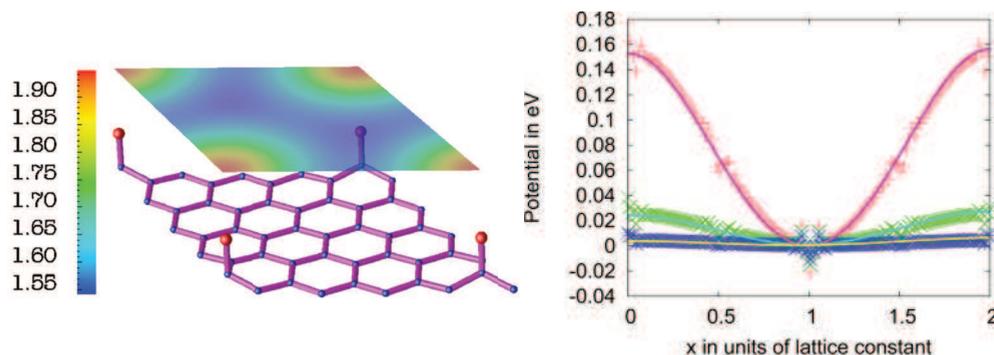
Fig. 1. Left: Periodic 4x4 graphene supercell with fluorine adsorbates (red dots). The contour plot shows the electrostatic potential (in eV) in a height of $z = 2a_{gr}$ (with $a_{gr} \approx 2.46\text{Å}$ the graphene lattice constant). To calculate the charge transfer, several paths through the cell are considered for different heights z and the image charge potential (Eqn. (1)) is fitted to the data by optimization of the parameters q_i. Right: Potential along paths connecting two adjacent chlorine adatoms on graphene 4x4 for heights $z = 3a_{gr}$ (red), $z = 4a_{gr}$ (green), $z = 5a_{gr}$ (blue) and fitted curves in units of the lattice constant; the curves are vertically shifted to the x-axis. Small noise occurs for certain x where a carbon atom is located.

The fitting parameters of this model are the adsorbate point charges q_i and an offset $V_e(z)$; the charges are centered at the positions of the impurity atoms, $\vec{r}_i = (x_i, y_i, z_i)$, and their mirror images $\vec{r}'_i = (x_i, y_i, -z_i)$. The offset is given by $V_e(z) = V_0 + E_0 z$, where V_0 is a constant and E_0 a constant electric field in z-direction due to the three-dimensional periodicity of the supercell.

The method proves well-suited to fit the charge values for all atomic adsorbates regarded. Merely for adsorbate groups like hydroxyl, additional dipole fields make the fitting procedure error-prone (sec. 3.2). Determining partial charges based on Eq. (1) is similar to analysing dipole moments obtained from the charge density as, e.g., performed for metal adatoms on graphene by Chan et al. (2008).

An alternative approach to charge transfer based on electrostatic potential is to analyse core potential shifts of the carbon atoms. These core level shifts arise from charge rearrangement around the impurity in the graphene sheet and can be calculated within VASP. The analysis of core level shifts allows estimates of the impurity charge and gives qualitative insight into the range of redistributions (Fig. 2). Within VASP, the averaged core potential for an atom sitting at position $\vec{R}_n$ is determined by (Kresse, 2010)

$$\overline{V}_n = \int V_{DFT}(\vec{r})\rho_{test}(|\vec{r} - \vec{R}_n|)d^3r, \tag{2}$$

where V_{DFT} denotes the electrostatic potential from DFT and ρ_{test} a test charge with norm 1 in the core region of each atom. This approach is similar to Adessi et al. (2006), where also atom centered test charges have been employed. The shift of these averaged core potentials, $\Delta\overline{V}$, as function of the distance to the bonding C atom is illustrated in Fig. 2.

Assuming screening within the linear response regime, the analysis of the core potentials allows to obtain the relative strength of charge transfer between the different adsorbates and graphene. If the charge transfer for one reference system is known, also absolute values for the charge transfer of all systems can be obtained. Additionally, the core potential shifts allow to

qualitatively characterize the spacial extent of doped regions. A detailed discussion of these issues will be given in sections 3.1, 3.2 and 3.3.
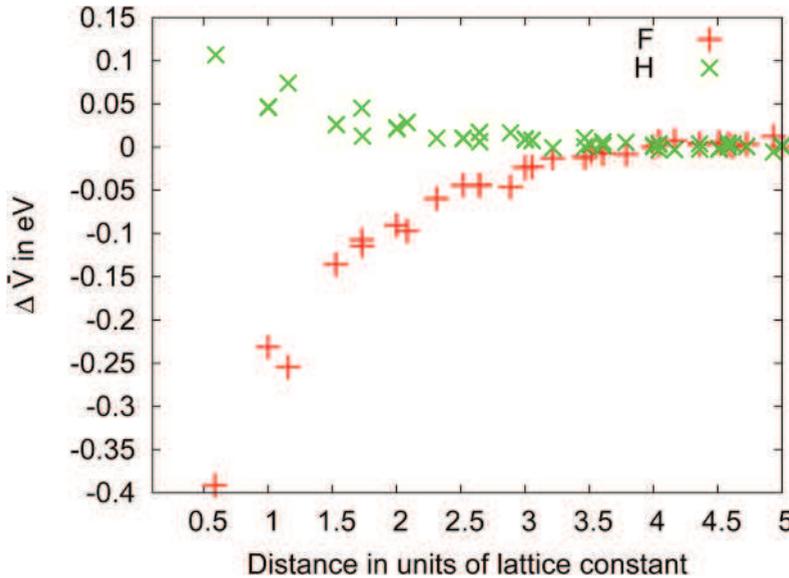

Fig. 2. Average core potential shift with respect to a C atom at large distance from the impurity as function of the in-plane distance for hydrogen and fluorine. The maximum distance considered, here, is about half the way through the supercell (here 4.5 lattice constants). It is visible that the doping of hydrogen is opposite to fluorine.

2.3 Band structure and density of states based determination of charge transfer

Spectroscopy experiments are a common tool to study the electronic structure of solids; in particular, these allow the determination of the density of states of graphene samples. Doping adsorbates donate or accept electrons from the graphene sheet, which leads to a shift of the Fermi level. This shift, the difference between the Fermi level E_F and the Dirac point energy E_D, is denoted by

$$\Delta E_F = E_F - E_D. \tag{3}$$

Note that in the case of pristine graphene, $E_F = E_D$, such that $\Delta E_F = 0$; the sign of ΔE_F denotes p- or n-type doping. Integrating the total density of states per unit cell of pristine graphene from E_D to $E_D + \Delta E_F$

$$\Delta q = e \int_{E_D}^{E_D + \Delta E_F} D(E) dE, \tag{4}$$

hence yields the charge transfer between the adsorbate and the graphene sheet which corresponds to a change in the number of mobile carriers. This method relies in the assumption that the adatoms do not change the density of states in the integration interval. While covalently bond adsorbates induce resonances in the DOS near the Dirac point (sec. 3.2), the method is well legitimate to apply for ionically bond impurities, where resonances only occur far away from the Dirac point ($\Delta E_F \leq 1.5 eV$; Fig. 3).
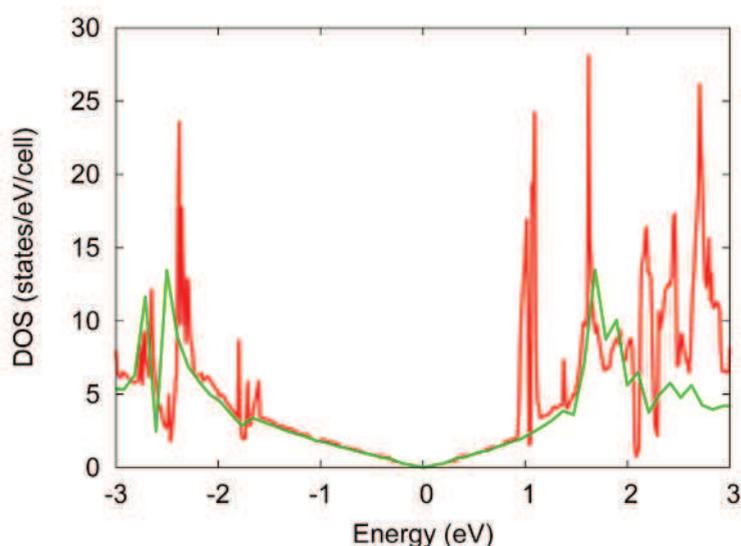
Fig. 3. Total density of states of pristine graphene (green) and of K on a graphene 4x4 supercell (red). The Fermi level is set to zero.

3. Monovalent adsorbates

We now consider monovalent adsorbates and show that these interact strongly with graphene. The charge transfer between the adsorbates and the graphene sheet is calculated by the approaches explained above and its relation to carrier doping as well as electron scattering is pointed out. The electronic structure of a graphene-impurity system features fundamental differences between covalently and ionically bond adsorbates; for instance, ARPES (angle-resolved photoemission spectroscopy) experiments yield that ionic potassium is a strong dopant with rather weak bond (Chen et al., 2008), while weak doping is found for covalent hydrogen in Raman experiments (Ryu et al., 2008). On this account, we will investigate doping processes with regard to the bonding mechanism and briefly point out reasons for the different bonding behaviour. In detail, calculations of monovalent hydrogen, fluorine, chlorine, potassium and hydroxyl adsorbed on graphene within DFT are presented in the following. Next to an extensive analysis of the charge transfer, we will discuss the range of charge redistributions with the help of a tight-binding model.

3.1 Ionically bond impurities

By definition, ionically bond impurites mean high charge transfer and low hybridization with the graphene bands. I.e. monovalent ionic adsorbates are expected to cause charge transfer in the range of $|q| \lesssim e$ [1]. This kind of charge transfer is detectable as a shift of the chemical potential in ARPES experiments (Ohta et al., 2006; Zhou et al., 2008). In the density of states, potassium and chlorine create a sharp resonance, which gives rise to an acceptor level below the Dirac point (Cl) or a donor level above (K; Fig. 3). The weak hybridization of the ionic impurities is also reflected in the migration barrier. These are typically in the range

---

[1] The reason for having $|q| \lesssim e$ instead of $|q| = e$, in a general case, lies in the fractional covalent character of any ionic bond.

Type	Size (conc.)	Image Charges	Core levels	Bader analysis	Fermi level shifts
K	4x4 (3.1%)	+0.68		+0.83	+0.64
	9x9 (0.6%)	+0.80	+0.80 (ref)	+0.91	+0.97
Cl	4x4 (3.1%)	-0.40		-0.50	-0.38
	9x9 (0.6%)	-0.54	-0.56	-0.57	-0.65

Table 1. Charge transfer between potassium / chlorine and graphene for the image charge model, the averaged core potential method, Bader analysis and the Fermi energy shifts in the DOS (all values in units of e) and two different supercell sizes (impurity concentrations). The value named "ref" for potassium is the charge value from the image charge method. It is used as a reference value to be able to extract absolute values for the charges of chlorine, hydrogen, fluorine and hydroxyl from the core levels.

of less than $0.1eV$ and therefore about one order smaller than for neutral covalent impurities (Wehling et al., 2009b).

We calculated charge transfer of potassium and chlorine adatoms by means of Bader analysis, in both electrostatic models and from Fermi level shifts. To this end, we fully relaxed the graphene adsorbate systems and obtained the minimum energy adsorption geometries (c.f. Wehling et al. (2009b)). Chlorine favours a top site (T) bonding (on top of a carbon atom) at 2.7Å above the graphene sheet, whereas potassium prefers the hollow site (H) in the middle of a carbon ring at a height of about 2.6Å.

In table 1 we present the charge transfer for both adsorbates obtained within the different approaches and as function of impurity concentration (supercell size). The signs of the partial charges show that potassium acts as a donor while chlorine behaves as an acceptor. The results for potassium are in rough agreement with Chan et al. (2008); they found a value of $0.76e$ for a 4x4 supercell, as well from Fermi level shifts. Similar findings were published by Lugo-Solis & Vasiliev (2007).

Obviously, the amount of charge transfer is concentration dependent: the strength of the doping decreases with the impurity concentration. This trend is consistently obtained within all methods to calculate charge transfer, here.

For the two ionic impurities all approaches are qualitatively consistent with each other. Depending on the experimental observable to be modelled either the electrostatic potential based methods or the Fermi level shifts should be considered. The values derived from the electrostatic potential should be most useful to discuss contribution to Coulomb scattering while the Fermi level shifts should yield quantitatively the best estimate of doping. The Bader results for ionically bond impurities tend to yield slightly higher charge values than the electrostatic models; covalent adsorbates, presented in the next section, are more problematic within this method.

3.2 Covalently bond impurities

In contrast to ionically bond impurities, covalent adsorbates show strong hybridization with graphene orbitals leading to a formation of stable states with strong bonds. The local density of states (LDOS) of covalently bond impurities is broad and constitutes a midgap state at the Fermi level as well as characteristic resonances at high energies (Wehling et al., 2009b).

All covalent monovalent adsorbates prefer top-site bonding and create impurity states that are localized at the adsorbate and the nearest neighbours of the bonding C atom (Fig. 4).

Type	Size (conc.)	Image Charges	Core level shifts	Bader analysis
H	4x4 (3.1%)	+0.18		+0.04
	5x5 (2.0%)	+0.16		+0.03
	7x7 (1.0%)	+0.14		+0.02
	9x9 (0.6%)	+0.15	+0.12	+0.01
F	4x4 (3.1%)	-0.39		-0.58
	5x5 (2.0%)	-0.39		-0.59
	6x6 (1.4%)	-0.38		-0.58
	9x9 (0.6%)	-0.39	-0.52	-0.57
OH	4x4 (3.1%)			-0.43
	5x5 (2.0%)			-0.45
	9x9 (0.6%)		-0.44	-0.45

Table 2. Charge transfer between hydrogen / fluorine / hydroxyl and graphene for the image charge model, the averaged core potential method and the Fermi energy shifts in the DOS and different different supercell sizes (impurity concentrations). All values in units of e.

The bonding partner of the impurity is decoupled from graphene's Dirac bands and scatters electrons similarly to vacancies. The universality of midgap states in graphene has been investigated by several groups (Boukhvalov & Katsnelson, 2009; Casolo et al., 2009; Wehling et al., 2008; 2009a;b).

We now turn to the description of charge redistributions due to covalent adsorbates. Their contribution to Coulomb scattering is directly related to changes in the electrostatic potential and consequently to the partial charges derived from the core level shifts or the image charge model. Our results for charge transfer within different models between graphene and hydrogen, fluorine, and hydroxyl adsorbates are given in table 2.

For hydrogen we obtain modulations in the electrostatic potential and the core levels corresponding to a "charge" as relevant for Coulomb scattering on the order of $0.1 - 0.2e$.
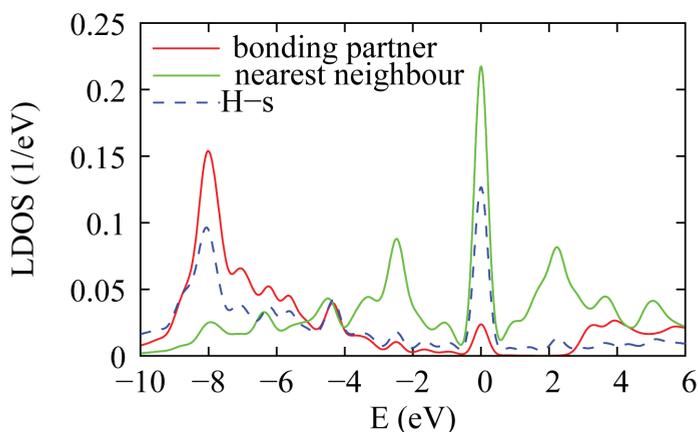

Fig. 4. Local density of states (LDOS) of hydrogen, the bonding partner, and the nearest neighbour on a 4x4 supercell (from Wehling et al. (2009b)).

Bader analysis yields a hydrogen partial charge of $q = 0.01 - 0.04e$. This is qualitatively consistent with the electrostatic models, as $|q| \ll e$ in both cases, but using the Bader charge in the context of Coulomb scattering would lead to an underestimation of the scattering strength. A hydrogen charge $|q| \ll e$ has also been obtained within Mulliken population analysis by Zhu et al. (2005).

Experimentally, the contribution of H adatoms on graphene to Coulomb scattering has not yet been determined. Ryu et al. (2008) investigated hydrogen doping effects by means of Raman spectroscopy. They estimate, under a hydrogen contamination saturating about 13% of carbon bonds (corresponding to approximately one hydrogen atom per 2x2 supercell), a charge donation of $0.003e$ per hydrogen atom. This is qualitatively in line with $|q| \ll e$ as obtained in the context of Coulomb scattering from DFT. However, it also demonstrates that an effective electrostatic charge on the order of $0.1 - 0.2e$ does not necessarily imply doping of the graphene bands by the same amount. As the LDOS in the vicinity of the Fermi level is significantly altered by the covalent adsorbates, Eq. (4) cannot be used to extract the doping from the DFT calculations.

Fluorine adatoms show covalent bonding, in contrast to the other groups VII elements (Wehling et al., 2009b). Due to the strong hybridization, the bonding carbon atom is lifted in z-direction by around 0.5Å. The fluorine adatom sits in a height of $z \approx 1.6$Å. Consistent with the large eletronegativity of F, the partial charge obtained within the electrostatic models (-0.4 — $-0.5e$) as well as by Bader analysis ($\sim -0.6e$) is significantly bigger than for H and correspondingly stronger Coulomb scattering due to F adsorbates is expected. The same holds for hydroxyl adsorbates which have been analysed within Bader and the averaged core potential method. Long range charge redistributions due to hydroxyl and fluorine will be further investigated within a tight-binding model in sec. 3.3.

Our charge analysis shows that the (electrostatic) charge of covalently bond adsorbates is rather constant in the range of impurity concentrations between 0.6% and 3%. This is in contrast to the ionically bond impurities, where charge transfer has been proven to increase with the supercell size.

3.3 Charge redistributions and coulomb interactions in a tight-binding model

To learn more about charge redistributions induced by covalent impurities in graphene we investigate this problem within a tight-binding (TB) model. For pristine graphene a TB model has been first considered by Wallace (1947). Concerning the question of charge rearrangement, the key benefit of this method lies in the possibility to calculate at much lower impurity concentrations than possible in full-potential DFT simulations. Supercells of a size up to around 100x100, thus concentrations of 0.005%, could be taken into account in our TB simulations.

Omitting the spin index and restricting to nearest-neighbour hopping, $t \approx 2.7eV$, the tight-binding Hamiltonian of pristine graphene reads

$$H_0 = -t \sum_{\langle i,j \rangle} \left(a_i^\dagger b_j + h.c. \right). \tag{5}$$

Here, $a_i(a_i^\dagger)$ and $b_i(b_i^\dagger)$ are the annihilation(creation) operators acting on electrons on site $\vec{R}_i$ in sublattice A or B.

In order to take impurity states into account, we extend the Hamiltonian by an orbital with on-site energy ϵ_{imp} which is coupled to a carbon atom orbital via the hopping V:

$$H = H_0 + V \left(a_{i'}^\dagger o + h.c. \right) + \epsilon_{imp} o^\dagger o. \tag{6}$$

Here, $o^\dagger$ (o) denotes the creation (annihilation) operator of an impurity adsorbed at a carbon atom of sublattice A on site $\vec{R}_{i'}$.

In order to simulate realistic impurities, one has to find accurate values for V and ϵ_{imp} first. This can be done by a fit of the tight-binding band structure to the DFT band structure of the considered graphene-impurity system (see e.g. Wehling et al. (2010)). In this section, we consider impurities with the parameters $V = 4.0eV$ and $\epsilon_{imp} = -2.0eV$ which roughly fit, both, the hydroxyl and the fluorine band structures from Wehling et al. (2009b). To investigate different adsorbate concentrations we simulate supercells of size $d \times d$ containing $2d^2$ carbon π orbitals and one impurity.

With the number operator $n_i = a_i^\dagger a_i$ and $n_i = b_i^\dagger b_i$ for i belonging to sublattice A and B, respectively, we consider the on-site occupancies $\rho_i = 2\langle n_i \rangle$ (the factor 2 is due to spin degeneracy) and its deviation

$$q_i = e(\rho_i - 1) \tag{7}$$

from the pristine graphene value. Analogously, we define for the impurity occupation $\rho_{imp} = 2\langle o^\dagger o \rangle$ and charge $q_{imp} = e(\rho_i - 1)$.

Table 3 gives the impurity charges, q_{imp}, obtained for different concentrations; it increases only slightly with the supercell size and saturates around $-0.6e$.

Partial impurity charge q_{imp} in units of e						
5x5	7x7	11x11	23x23	37x37	61x61	83x83
-0.341	-0.344	-0.431	-0.536	-0.573	-0.588	-0.591

Table 3. Charge transfer to the hydroxyl group within tight-binding.

The impurity charges obtained in the TB model mimicking hydroxyl or fluorine are in qualitative agreement with the strength of the Coulomb potentials extracted from core potential shifts in section (3.2).

The lateral extent of the doped regions can be studied by constructing a circular disk of radius r_d around the impurity and summing up all partial charges of the atoms within the disk, including the impurity. The total disk charge is given by

$$q_{disk} = q_{imp} + \sum_{i \in \{ |\vec{R}_0 - \vec{R}_i| \le r_d \}} q_i \tag{8}$$

where $\vec{R}_0$ is the lateral position of the impurity, $\vec{R}_i$ the position of the carbon atom at site i. For different disk radii, the total charge can be obtained from the model and the range of redistributions estimated (Fig. 5, right).

In the region of the impurity, the sign of the on-site partial charge allows clear distinction between the sublattices (Fig. 5, left). With impurity binding to a sublattice A atom, the A sublattice is hole-doped, while the B sublattice is electron-doped near the impurity and slightly hole-doped far away. In close proximity to the impurity, the disk is charged by the adatom and a maximum in the disk charge due to the midgap impurity state occurs within
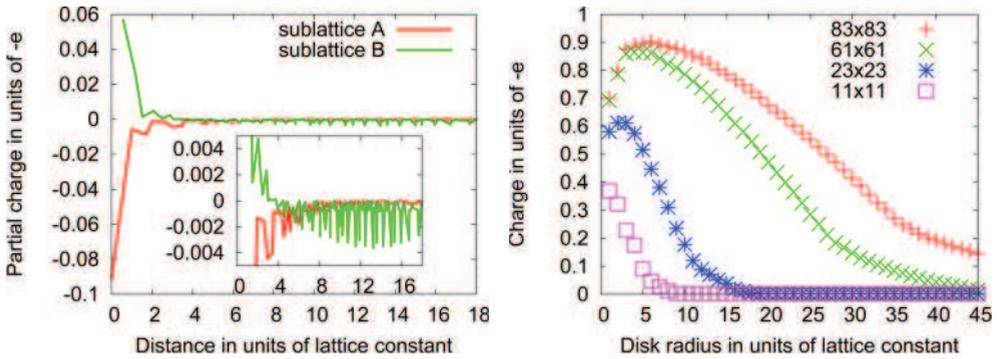
Fig. 5. Hydroxyl in nn TB: Partial charges of graphene atoms on sublattice A (red) and B (green) for a 23x23 supercell as function of the distance (left) together with a zoom (inset). The total disk charge for several supercell sizes is shown right.

some lattice constants off the impurity. For larger supercells, i.e. lower concentrations of impurities, the maximum disk charge increases (Fig. 5, right); the slope of the disk charge is simply given by the single partial charges (Fig. 5, left) which show small Friedel oscillations. Far away from the impurity, the B sublattice is charged negatively such that the total disk charge decreases almost linearly. We note that the range of charge redistributions (region with linear slope in Fig. 5, right) is on the order of the inter impurity distance even for impurity concentrations as low as 0.007% corresponding to the 83×83 supercell.

Concerning long-range doping, the question of a possible oversimplification of the TB model arises. In reality, the Coulomb energy cost might suppress long range charge redistributions. Therefore, we extend the Hamiltonian (6) by an additional term, taking electrostatic interaction between all N electrons into account (Castro Neto et al., 2009):

$$H_C = \frac{1}{2} \sum_{i,j} U_{i,j} n_i n_j. \tag{9}$$

The term $U_{i,j}$ describes the Coulomb repulsion

$$U_{i,j} = \frac{e^2}{4\pi\epsilon_0 |\vec{R}_i - \vec{R}_j|} \tag{10}$$

between two electrons on different sites ($\vec{R}_i \neq \vec{R}_j$). The on-site repulsion was chosen to $U_{ii} = 15eV$. We solve the Hamiltonian $H + H_C$ within the Hartree approximation, wherein the many-body electron-electron interaction (9) is replaced by the electrostatic potential from charge distribution in the system. Hence, we replace (9) by the Hartree Hamiltonian

$$H_H = \sum_i^N V_i n_i \tag{11}$$

with

$$V_i = \sum_j^N U_{i,j} \langle n_j \rangle. \tag{12}$$

The problem is solved self-consistently; after the initial determination of an eigensystem from Hamiltonian (6), the Coulomb part (11) is calculated and the eigensystem updated; this procedure is repeated until a converged solution is obtained.
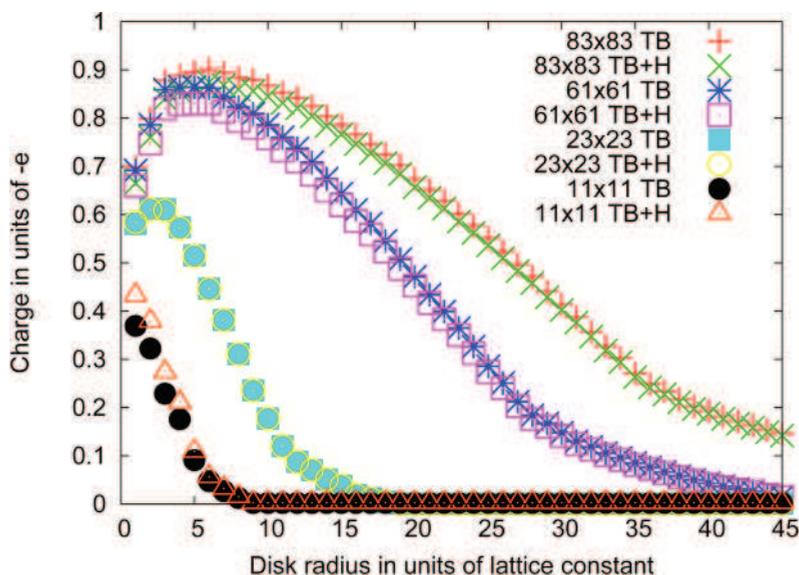

Fig. 6. Charge of the disk around the adsorbate as function of the radius for OH on graphene. The plot shows curves for different supercell sizes A (see legend); "TB" calculations are performed in nn tight-binding without Coulomb repulsion, "TB+H" curves are from nn tight-binding with Coulomb interaction in Hartree approximation.

The results for the impurity with $V = 4.0eV$ and $\epsilon_{imp} = -2.0eV$ show that the long range Coulomb interaction does not significantly affect the charge distribution in the doped region (Fig. 6). For supercells larger than 23x23, the Coulomb repulsion tends to slightly reduce the disk charges, whereas for small supercells, i.e. high concentrations, the charges slightly increase. The transfer between adsorbate and graphene layer only changes insignificantly, such that Coulomb interactions keep charge transfer and redistribution almost unaffected in the window of investigated impurity concentrations from 0.007% to 2%.

4. Conclusions

In this chapter we investigated adsorption processes under the general aspect of charge transfer. Charge transfer can either refer to doping, i.e. from electrons transferred from states localized at the impurity to the host bands, or to the redistribution of charge density associated electrostatic potentials. These two types of charge transfer have to be carefully distinguished. The electrostatic potentials due to charge redistributions are particularly important in the context of Coulomb scattering. We investigated charge transfer of realistic monovalent adsorbates on graphene by electrostatic means, i.e. the image charge method and core level shifts, and derived the effective charge q of the impurities to be used in the context of Coulomb scattering. For ionic impurities we find effective charges on the order of $|q| \sim 0.5 - 1e$

and for covalent impurities $|q|$ in the range of $0.0 - 0.5e$. Hydrogen adatoms which are of particular experimental importance create electrostatic fields corresponding to a partial charge of $q \approx 0.1e$.

For the ionic impurities the graphene bands remain mainly intact and the doping can be estimated from the position of the Fermi level with respect to the Dirac point. Qualitatively, the impurity charges obtained in this method for K and Cl coincide with the respective effective charges in the context of Coulomb scattering. Moreover, the charge transfer of ionic potassium and chlorine proved to be similarly and consistently sensitive to the impurity concentration, both, in the context of doping as well as Coulomb scattering. There are, however, quantitative differences between the charge as relevant for Coulomb scattering and for doping. The latter turned out to be up to 20% bigger than the former.

Further investigated charge redistributions within the graphene sheet by means of a tight-binding describe impurities like hydroxyl or fluorine. The model illustrates that even far away from the impurity and for low impurity concentrations rearrangement of electrons is detectable. These results hold true if Coulomb repulsion is taken into account. The impurity charge in the TB model is in qualitative agreement with the charge transfer obtained from the core potential method applied to the DFT data of hydroxyl or fluorine adsorbates.

In the future, the contribution of different realistic adsorbates to minimum carrier concentrations achievable in graphene would be worth to investigate. Moreover, interfacing the charge transfer with electron transport theory would be desirable and might be a key to a realistic first-principles based theory of electron transport in graphene.

5. Acknowledgement

6. References

Adam, S., Hwang, E., Galitski, V. & Das Sarma, S. (2007). A self-consistent theory for graphene transport, *Proceedings of the National Academy of Sciences* 104(47): 18392.

Adessi, C., Roche, S. & Blase, X. (2006). Reduced backscattering in potassium-doped nanotubes: Ab initio and semiempirical simulations, *Physical Review B* 73(12): 125414.

Bader, R. (1991). A quantum theory of molecular structure and its applications, *Chemical Reviews* 91(5): 893–928.

Bolotin, K. I., Sikes, K. J., Jiang, Z., Klima, M., Fudenberg, G., Hone, J., Kim, P. & Stormer, H. L. (2008). Ultrahigh electron mobility in suspended graphene, *Solid State Commun.* 146: 351.

Bostwick, A., Ohta, T., Seyller, T., Horn, K. & Rotenberg, E. (2006). Quasiparticle dynamics in graphene, *Nature Physics* 3(1): 36–40.

Boukhvalov, D. & Katsnelson, M. (2009). Enhancement of chemical activity in corrugated graphene, *The Journal of Physical Chemistry C* 113(32): 14176–14178.

Casolo, S., Løvvik, O., Martinazzo, R. & Tantardini, G. (2009). Understanding adsorption of hydrogen atoms on graphene, *The Journal of chemical physics* 130: 054704.

Castro Neto, A., Guinea, F., Novoselov, K. & Geim, A. (2009). The electronic properties of graphene, *Rev. Mod. Phys.* 81(1): 109.

Chan, K., Neaton, J. & Cohen, M. (2008). First-principles study of metal adatom adsorption on graphene, *Phys. Rev. B* 77(23): 235430.

Chen, J.-H., Cullen, W. G., Jang, C., Fuhrer, M. S. & Williams, E. D. (2009). Defect scattering in graphene, *Phys. Rev. Lett.* 102(23): 236805.

Chen, J.-H., Jang, C., Adam, S., Fuhrer, M., Williams, E. D. & Ishigami, M. (2008). Charged-impurity scattering in graphene, *Nature Physics* 4(5): 377–381.

Cheng, S.-H., Zou, K., Okino, F., Gutierrez, H. R., Gupta, A., Shen, N., Eklund, P. C., Sofo, J. O. & Zhu, J. (2010). Reversible fluorination of graphene: Evidence of a two-dimensional wide bandgap semiconductor, *Phys. Rev. B* 81(20): 205435.

Collins, P., Bradley, K., Ishigami, M. & Zettl, A. (2000). Extreme oxygen sensitivity of electronic properties of carbon nanotubes, *Science* 287(5459): 1801.

Du, X., Skachko, I., Barker, A. & Andrei, E. Y. (2008). Approaching ballistic transport in suspended graphene, *Nat. Nano.* 3: 491–495.

Elias, D., Nair, R., Mohiuddin, T., Morozov, S., Blake, P., Halsall, M., Ferrari, A., Boukhvalov, D., Katsnelson, M., Geim, A. et al. (2009). Control of graphene's properties by reversible hydrogenation: evidence for graphane, *Science* 323(5914): 610.

Geim, A. & Novoselov, K. (2007). The rise of graphene, *Nature Materials* 6(3): 183–191.

Hwang, E., Adam, S. & Das Sarma, S. (2007). Carrier transport in two-dimensional graphene layers, *Phys. Rev. Lett.* 98(18): 186806.

Katoch, J., Chen, J., Tsuchikawa, R., Smith, C., Mucciolo, E., Ishigami, M., Chung, S., Qi, X., Maciejko, J., Zhang, S. et al. (2010). Uncovering the dominant scatterer in graphene sheets on SiO2, *Phys. Rev. B* 82(8): 81417.

Katsnelson, M. (2006). Nonlinear screening of charge impurities in graphene, *Physical Review B* 74(20): 201401.

Katsnelson, M. (2007). Graphene: carbon in two dimensions, *Materials Today* 10(1-2): 20 – 27.

Katsnelson, M. & Novoselov, K. (2007). Graphene: new bridge between condensed matter physics and quantum electrodynamics, *Solid State Communications* 143(1-2): 3–13.

Kong, J., Franklin, N., Zhou, C., Chapline, M., Peng, S., Cho, K. & Dai, H. (2000). Nanotube molecular wires as chemical sensors, *Science* 287(5453): 622.

Kresse, G. (2010). VASP the GUIDE. http://cms.mpi.univie.ac.at/vasp/vasp/ LVTOT_tag_core_level_shifts.html, accessed 24-Sept-2010.

Kresse, G. & Furthmüller, J. (1996a). Efficiency of ab-initio total energy calculations for metals and semiconductors using a plane-wave basis set, *Computational Materials Science* 6(1): 15–50.

Kresse, G. & Furthmüller, J. (1996b). Efficient iterative schemes for ab initio total-energy calculations using a plane-wave basis set, *Phys. Rev. B* 54(16): 11169–11186.

Lebègue, S., Klintenberg, M., Eriksson, O. & Katsnelson, M. I. (2009). Accurate electronic band gap of pure and functionalized graphane from GW calculations, *Phys. Rev. B* 79(24): 245117.

Leenaerts, O., Partoens, B. & Peeters, F. (2008). Paramagnetic adsorbates on graphene: A charge transfer analysis, *Applied Physics Letters* 92: 243125.

Liu, L. & Shen, Z. (2009). Bandgap engineering of graphene: A density functional theory study, *Applied Physics Letters* 95: 252104.

Lugo-Solis, A. & Vasiliev, I. (2007). Ab initio study of K adsorption on graphene and carbon nanotubes: Role of long-range ionic forces, *Phys. Rev. B* 76(23): 235431.

Meister, J. & Schwarz, W. H. E. (1994). Principal Components of Ionicity, *J. Phys. Chem.* 98: 8245–8252.

Meyer, J., Girit, C., Crommie, M. & Zettl, A. (2008). Imaging and dynamics of light atoms and molecules on graphene, *Nature* 454(7202): 319–322.

Moser, J., Verdaguer, A., Jiménez, D., Barreiro, A. & Bachtold, A. (2008). The environment of graphene probed by electrostatic force microscopy, *Applied Physics Letters* 92: 123507.

Nair, R. R., Ren, W. C., Jalil, R., Riaz, I., Kravets, V. G., Britnell, L., Blake, P., Schedin, F., Mayorov, A. S., Yuan, S., Katsnelson, M. I., Cheng, H. M., Strupinski, W., Bulusheva, L. G., Okotrub, A. V., Grigorieva, I. V., Grigorenko, A. N., Novoselov, K. S. & Geim, A. K. (2010). Fluorographene: Two Dimensional Counterpart of Teflon, *ArXiv preprint arXiv:1006.3016* .

Ni, Z., Ponomarenko, L., Nair, R., Yang, R., Grigorieva, S., Schedin, F., Shen, Z., Hill, E., Novoselov, K. & Geim, A. (2010). On resonant scatterers as a factor limiting carrier mobility in graphene, *Arxiv preprint arXiv:1003.0202* .

Nomura, K. & MacDonald, A. H. (2006). Quantum hall ferromagnetism in graphene, *Phys. Rev. Lett.* 96(25): 256602.

Novoselov, K., Geim, A., Morozov, S., Jiang, D., Zhang, Y., Dubonos, S., Grigorieva, I. & Firsov, A. (2004). Electric Field Effect in Atomically Thin Carbon Films, *Science* 306(5696): 666–669.

Ohta, T., Bostwick, A., Seyller, T., Horn, K. & Rotenberg, E. (2006). Controlling the electronic structure of bilayer graphene, *Science* 313(5789): 951.

Ostrovsky, P. M., Gornyi, I. V. & Mirlin, A. D. (2006). Electron transport in disordered graphene, *Phys. Rev. B* 74(23): 235443.

Peres, N. M. R. (2010). Colloquium: The transport properties of graphene: An introduction, *Rev. Mod. Phys.* 82(3): 2673–2700.

Robinson, J., Perkins, F., Snow, E., Wei, Z. & Sheehan, P. (2008). Reduced graphene oxide molecular sensors, *Nano letters* 8(10): 3137–3140.

Robinson, J., Schomerus, H., Oroszlány, L. & Fal'ko, V. (2008). Adsorbate-Limited Conductivity of Graphene, *Phys. Rev. Lett.* 101(19): 196803.

Robinson, J. T., Burgess, J. S., Junkermeier, C. E., Badescu, S. C., Reinecke, T. L., Perkins, F. K., Zalalutdniov, M. K., Baldwin, J. W., Culbertson, J. C., Sheehan, P. E. & Snow, E. S. (2010). Properties of fluorinated graphene films, *Nano Letters* 10(8): 3001–3005.

Ryu, S., Han, M., Maultzsch, J., Heinz, T., Kim, P., Steigerwald, M. & Brus, L. (2008). Reversible basal plane hydrogenation of graphene, *Nano Lett* 8(12): 4597–4602.

Schedin, F., Geim, A., Morozov, S., Hill, E., Blake, P., Katsnelson, M. & Novoselov, K. (2007). Detection of individual gas molecules adsorbed on graphene, *Nature materials* 6(9): 652–655.

Segall, M. D., Pickard, C. J., Shah, R. & Payne, M. C. (1996). Population analysis in plane wave electronic structure calculations, *Mol. Phys.* 89: 571.

Sofo, J., Chaudhari, A. & Barber, G. (2007). Graphane: A two-dimensional hydrocarbon, *Phys. Rev. B* 75(15): 153401.

Stauber, T., Peres, N. M. R. & Guinea, F. (2007). Electronic transport in graphene: A semiclassical approach including midgap states, *Phys. Rev. B* 76(20): 205423.

Tan, Y., Zhang, Y., Bolotin, K., Zhao, Y., Adam, S., Hwang, E., Das Sarma, S., Stormer, H. & Kim, P. (2007). Measurement of scattering rate and minimum conductivity in graphene, *Phys. Rev. Lett.* 99(24): 246803.

Wallace, P. (1947). The Band Theory of Graphite, *Phys. Rev.* 71(9): 622–634.

Wehling, T., Balatsky, A., Tsvelik, A., Katsnelson, M. & Lichtenstein, A. (2008). Midgap states in corrugated graphene, *EPL (Europhysics Letters)* 84: 17003.

Wehling, T., Katsnelson, M. & Lichtenstein, A. (2009a). Adsorbates on graphene: Impurity states and electron scattering, *Chemical Physics Letters* 476(4-6): 125 – 134.

Wehling, T., Katsnelson, M. & Lichtenstein, A. (2009b). Impurities on graphene: Midgap states and migration barriers, *Phys. Rev. B* 80(8): 085428.

Wehling, T., Yuan, S., Lichtenstein, A., Geim, A. & Katsnelson, M. (2010). Resonant scattering by realistic impurities in graphene, *Phys. Rev. Lett.* 105(5): 056802.

Xiang, H., Kan, E., Wei, S., Whangbo, M. & Yang, J. (2009). "Narrow" Graphene Nanoribbons Made Easier by Partial Hydrogenation, *Nano letters* 9(12): 4025–4030.

Zhou, S., Siegel, D., Fedorov, A. & Lanzara, A. (2008). Metal to Insulator Transition in Epitaxial Graphene Induced by Molecular Doping, *Phys. Rev. Lett.* 101(8): 086402.

Zhu, Z., Lu, G. & Wang, F. (2005). Why H atom prefers the on-top site and alkali metals favor the middle hollow site on the basal plane of graphite, *J. Phys. Chem. B* 109(16): 7923–7927.
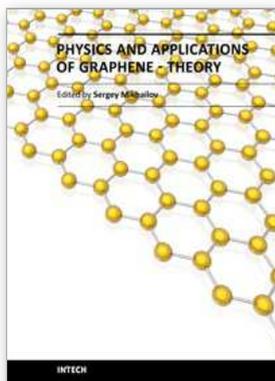
Physics and Applications of Graphene - Theory
Edited by Dr. Sergey Mikhailov

The Stone Age, the Bronze Age, the Iron Age... Every global epoch in the history of the mankind is characterized by materials used in it. In 2004 a new era in material science was opened: the era of graphene or, more generally, of two-dimensional materials. Graphene is the strongest and the most stretchable known material, it has the record thermal conductivity and the very high mobility of charge carriers. It demonstrates many interesting fundamental physical effects and promises a lot of applications, among which are conductive ink, terahertz transistors, ultrafast photodetectors and bendable touch screens. In 2010 Andre Geim and Konstantin Novoselov were awarded the Nobel Prize in Physics "for groundbreaking experiments regarding the two-dimensional material graphene". The two volumes Physics and Applications of Graphene - Experiments and Physics and Applications of Graphene - Theory contain a collection of research articles reporting on different aspects of experimental and theoretical studies of this new material.

How to reference
In order to correctly reference this scholarly work, feel free to copy and paste the following:

B. Sachs, T.O. Wehling, A. I. Lichtenstein and M. I. Katsnelson (2011). Theory of Doping: Monovalent Adsorbates, Physics and Applications of Graphene - Theory, Dr. Sergey Mikhailov (Ed.), ISBN: 978-953-307-152-7, InTech, Available from: http://www.intechopen.com/books/physics-and-applications-of-graphene-theory/theory-of-doping-monovalent-adsorbates

INTECH
open science | open minds